Wetting on spherical and cylindrical substrates: Global phase diagrams

P. J. Upton* and J. O. Indekeu
Laboratorium voor Molekuulfysika, Katholieke Universiteit Leuven, B-3030 Leuven, Belgium

J. M. Yeomans
Department of Theoretical Physics, 1 Keble Road, Oxford OX1 3NP, England
(Received 21 November 1988)

A Landau theory for wetting on spherical and cylindrical substrates is studied. The substrate parameters are the radius r_1, the surface field h_1, and the surface-coupling enhancement g. The adsorbate is characterized by correlation length ξ and critical temperature T_c. The global phase diagrams reveal important features which were omitted in previous works. For $T < T_c$, the phase diagrams are obtained numerically and with use of analytic approximations. For $T \geq T_c$, they are obtained exactly. For $T < T_c$, there are two distinct regimes of adsorption phase transitions: The regime $\xi \lesssim r_1 \leq \infty$ where the curvature of the substrate is small and the adsorbate is away from criticality, and the regime $0 < r_1 \lesssim \xi$ where the curvature is high and the adsorbate is near-critical. In the former regime, the phase transitions are referred to as "surface" transitions, and in the latter regime as "point" transitions (for spheres) and "line" transitions (for cylinders). The two regimes merge at a critical double point in the phase diagram. Beyond this point adsorption phase transitions can occur for arbitrary curvature and for all temperatures, including T_c. The wetting layer thicknesses behave as $\xi \ln(r_1/\xi)$ for $r_1 \gg \xi$ and as ξ for $r_1 \ll \xi$. The finite-size rounding of the phase transitions is discussed, and the experimental relevance of our findings is outlined.

I. INTRODUCTION AND GLOBAL PHASE DIAGRAMS

The wetting transition on planar substrates is now well understood.[1–5] However, considerably less attention has been paid to less obvious substrate geometries. Our aim in this paper is to consider wetting on (the outside of) spherical and cylindrical substrates.[5–9] We shall show that several novel features appear, and we present the global surface phase diagrams within Landau theory. We will not consider the complementary subject of wetting inside spherical cavities or cylindrical pores, which involves capillary condensation.[5]

An interface bound to a spherical or cylindrical substrate cannot unbind to infinity because the increase in its area leads to an unbounded positive contribution to the free energy of the system. Hence any phase transition must be between a thin and a thick wetting layer. This is analogous to wetting in flat geometries in the presence of a symmetry-breaking bulk field (prewetting),[1] or in the presence of a long-range surface field which favors drying (competing forces).[10,11] Since true wetting cannot occur on spheres or cylinders we will refer to possible phase transitions as *adsorption phase transitions.* This terminology will turn out to be useful below, at, and above the bulk critical temperature T_c of the adsorbate. (Note that inside spheres and cylinders true wetting cannot occur either, because the phenomenon is overpowered by capillary condensation.)

In our study we employ the Landau theory with the standard quartic polynomial for the bulk free energy. For $T \geq T_c$, we obtain the exact critical line bounding the region of first-order adsorption phase transitions for both spherical and cylindrical substrates. For $T < T_c$ the critical line is obtained numerically and then checked using exact inequalities as well as an analytic expansion valid for weakly varying order-parameter profiles. The natural variables in our problem are a "temperature" or "inverse-curvature" variable r_1/ξ, with r_1 the substrate radius and ξ the bulk correlation length of the adsorbate, and a "surface-coupling enhancement" variable G.

Our results are best summarized by Figs. 1, 2, and 3, which present the global phase diagrams for the spherical, cylindrical, and planar substrates, respectively. We denote the bulk correlation length by ξ_- or ξ_+, for $T < T_c$ or $T > T_c$, respectively. For dehanced surface couplings ($G < 0$) on spheres or cylinders adsorption phase transitions can only occur when T is sufficiently below T_c. By contrast, on planar substrates wetting phase transitions can occur for all $T < T_c$, as first-order phase transitions for T sufficiently below T_c, and as second-order ones for T closer to T_c. The region of critical wetting (Fig. 3) is absent for spheres and cylinders, and wetting *tricriticality* on planes becomes adsorption *criticality* on the curved substrates. For enhanced surface couplings ($G > 0$) on spheres or cylinders, the phase diagrams feature a *critical double point,* where the tangent to the critical line is vertical. When G is greater than its value at the critical double point, adsorption phase transitions can occur for arbitrary temperatures (below, at, and above T_c), and for arbitrary curvatures.

For $\xi \lesssim r_1 < \infty$ the substrate curvature is effectively small and we refer to adsorption phase transitions in this regime as *surface transitions.* On the other hand, for

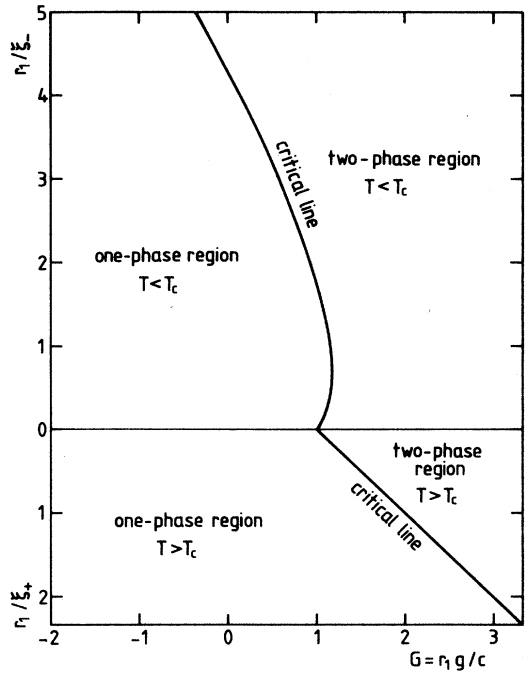

FIG. 1. Global phase diagram for wetting on spherical substrates in the plane of inverse curvature r_1/ξ and substrate coupling enhancement G. For $T<T_c$, ξ is denoted by ξ_-, and for $T>T_c$, by ξ_+. The two-phase regions of adsorption phase transitions are bounded by critical lines which meet at $T=T_c$ and $G=1$. Note, for $T<T_c$, the presence of a critical double point where the tangent to the critical line is vertical. There, the regions of "surface" transitions ($\xi \lesssim r_1 \leq \infty$) and "point" transitions ($0<r_1 \lesssim \xi$) separate as G is decreased.

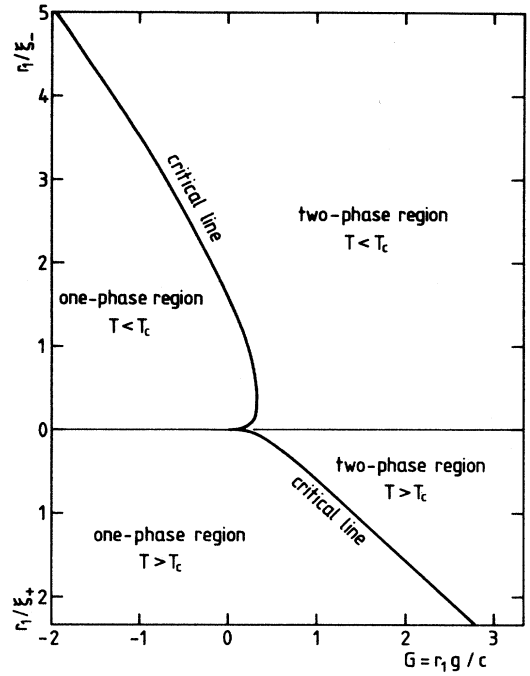

FIG. 2. Global phase diagram for wetting on cylindrical substrates in the plane of inverse curvature r_1/ξ and substrate coupling enhancement G. The critical lines meet with horizontal tangents at $T=T_c$ and $G=0$. Note, for $T<T_c$, the presence of a critical double point where the regions of "surface" transitions ($\xi \lesssim r_1 \leq \infty$) and "line" transitions ($0<r_1 \lesssim \xi$) separate as G is decreased.

$0<r_1 \lesssim \xi$, that is the high-curvature regime (or, equivalently, close to T_c), we refer to them as *point transitions* (spheres) and *line transitions* (cylinders). This nomenclature is inspired by the fact that, for $r_1 \to \infty$ (planar limit), the transitions correspond to singularities in a surface free energy, whereas, for fixed r_1, they correspond to singularities in a point or line free energy (within Landau theory). Furthermore, in the regime $r_1 \ll \xi$, the wetting layer thickness (of order ξ) can become arbitrarily large with respect to the substrate radius. This is qualitatively different from the planar limit where the layer thickness is controlled by the substrate radius.

Note that in a restricted range of positive values of G, the regions of surface and point (or line) transitions are separated by a one-phase region (which terminates at the critical double point). When the curvature is increased from a sufficiently low value, the phase transition terminates at a critical point, but the phase transition reappears when the curvature is increased further, via a second critical point.

The global phase diagrams for spheres and cylinders present new and unexpected topologies, the more so because previous studies produced an incomplete phase diagram topology by applying the double-parabola approxi-

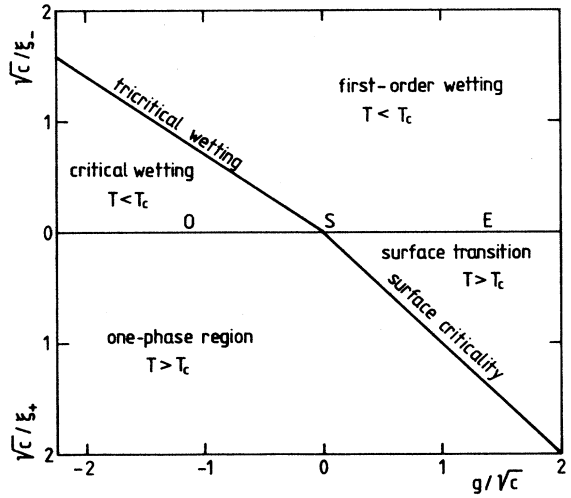

FIG. 3. Global phase diagram for wetting on planar substrates. This phase diagram results from the phase diagrams for spherical or cylindrical substrates in the limit $r_1 \to \infty$. For $T<T_c$, a region of first-order wetting transitions meets a region of critical (second-order) wetting transitions, at a line of tricritical wetting transitions. For $T>T_c$, a two-phase region of "pure" surface transitions is bounded by a critical line. At T_c, we distinguish the ordinary transition O ($g<0$), the extraordinary transition E ($g>0$), and the special transition S ($g=0$). Note how this rich phase diagram with simple geometry is modified for curved substrates (Figs. 1 and 2).

mation in the Landau theory.[9] In contrast, the early work by Levinson *et al.* consisted of an accurate numerical approach to the Landau theory.[6] However, in that study attention was restricted to the special case $G=0$.

The plan of the paper is as follows. In Sec. II the Landau surface free-energy functional is defined and the differential equations and associated boundary conditions describing wetting on spherical and cylindrical substrates are derived, for $T<T_c$. Section III describes numerical results for $T<T_c$, and Sec. IV discusses an analytic approximation and exact inequalities for $T<T_c$. In Sec. V exact results are obtained for $T>T_c$, and in Sec. VI the case $T=T_c$ is treated exactly with the use of inequalities. The behavior of the surface field h_1 along the critical line of the adsorption transitions, in the vicinity of T_c, is examined in Sec. VII by means of analytic approximations. The phenomena which occur when the adsorbate is taken off bulk coexistence because of the presence of a bulk field h, are studied in Sec. VIII, which deals with prewetting. Section IX focusses on the wetting layer thicknesses, which behave as $\xi\ln(r_1/\xi)$ for $r_1\gg\xi$, and as ξ for $r_1\ll\xi$. In Sec. X the issue of the finite-size rounding of the adsorption phase transition is addressed, and Sec. XI closes the paper with a discussion and outlook.

A preliminary account of our main results for wetting on cylinders has been published.[12]

II. DERIVATION OF THE DIFFERENTIAL EQUATIONS FOR $T<T_c$

We shall illustrate the derivation of the differential equation that describes the order parameter profile for the case of spheres. Consider a sphere of radius r_1 immersed in a fluid at two-phase coexistence. The usual Landau surface free-energy functional is

$$\gamma[m]=\frac{1}{r_1^2}\int_{r_1}^{\infty}dr\,r^2\left[\frac{c}{2}\left[\frac{dm}{dr}\right]^2+f(m(r))\right]+\gamma_s(m_1)\ , \tag{2.1}$$

where $m(r)$ is the order-parameter profile for $r\geq r_1$, and $m_1\equiv m(r_1)$. The bulk free-energy density is given as usual by

$$f(m(r))=a_0+a_2m^2+a_4m^4\ , \tag{2.2}$$

and we take $a_4=1$, $a_2=2(T-T_c)$, and a_0 such that $\min[f(m)]=0$. The bulk order-parameter values, $\pm m_b$, at coexistence ($T\leq T_c$) are then given by $m_b^2=T_c-T$. For the substrate-adsorbate energy the standard choice is

$$\gamma_s(m_1)=-h_1m_1-g\frac{m_1^2}{2}\ , \tag{2.3}$$

where h_1 is a surface field and g a surface-coupling enhancement.

It is convenient to use scaled variables

$$\rho=r/r_1,\quad x=x(\rho)=m(r)/m_b \tag{2.4}$$

in terms of which the free-energy functional becomes

$$\Gamma[x]\equiv r_1\gamma[m]/(cm_b^2) \tag{2.5}$$

$$=\int_1^{\infty}d\rho\,\rho^2\left[\frac{1}{2}\left[\frac{dx}{d\rho}\right]^2+\frac{\Omega}{4}(x^2-1)^2\right]-H_1x_1-G\frac{x_1^2}{2} \tag{2.6}$$

$$\equiv D[x]+\Gamma_s(x_1)\ , \tag{2.7}$$

where

$$H_1=r_1h_1/(cm_b),\quad G=r_1g/c\ , \tag{2.8}$$

and

$$\Omega=4r_1^2m_b^2/c=(r_1/\xi)^2\ , \tag{2.9}$$

introducing the bulk correlation length $\xi=c^{1/2}/(2m_b)$, or, more generally, $\xi=c^{1/2}/(2|T-T_c|^{1/2})$.

Extremization of (2.6) leads to the Euler-Lagrange equation

$$\ddot{x}+2\frac{\dot{x}}{\rho}=\Omega x(x^2-1)\ , \tag{2.10}$$

where $\dot{x}\equiv dx/d\rho$, etc., or, equivalently,

$$\dot{x}=-y\ , \tag{2.11a}$$

$$\dot{y}=-\frac{2y}{\rho}-\Omega x(x^2-1)\ , \tag{2.11b}$$

together with the boundary condition at the substrate,

$$y_1=H_1+Gx_1\ . \tag{2.12}$$

Finally, as $\rho\to\infty$, the system is assumed to be in the bulk vapor phase,

$$x_\infty=-1\ . \tag{2.13}$$

The equations for a cylindrical substrate can be derived in an exactly analogous way. Minimization of a surface free-energy functional

$$\gamma[m]=\frac{1}{r_1}\int_{r_1}^{\infty}dr\,r\left[\frac{c}{2}\left[\frac{dm}{dr}\right]^2+f(m(r))\right]+\gamma_s(m_1) \tag{2.14}$$

gives the differential equation

$$\ddot{x}+\frac{\dot{x}}{\rho}=\Omega x(x^2-1)\ , \tag{2.15}$$

which is solved subject to the same boundary conditions (2.12) and (2.13).

Note that in a mechanical analogy of our problem (position x, time ρ), Eqs. (2.10) and (2.15) represent the equation of motion under a nonlinear force and time-dependent friction. At time infinity the particle is required to come to a stop on the summit of a potential hill.

III. NUMERICAL RESULTS FOR $T<T_c$

Our aim is to search for first-order adsorption phase transitions in the space $(r_1/\xi,G,H_1)$. Because of an

equal-areas rule such transitions can be predicted from a knowledge of the geometry of $y_1(x_1)$, the curve of allowed initial conditions which is determined for a spherical substrate by

$$\frac{y_1^2}{2}=\frac{\Omega}{4}(x_1^2-1)^2+2\int_{-1}^{x_1}\frac{y}{\rho}dx \ , \tag{3.1}$$

as follows from (2.11b).

Numerically the curve of initial conditions can be obtained for a given Ω by iterating (2.11). $y_1(x_1)$ are then the values which give the correct boundary condition, (2.13), as $\rho\to\infty$.

The equal-areas rule follows from considering the free-energy functional $\Gamma[x]$ for profiles satisfying (2.10) and (2.13) as a *function* of x_1, say $\tilde{\Gamma}(x_1)=\tilde{D}(x_1)+\Gamma_s(x_1)$ [cf. (2.7)]. Extremization of $\tilde{\Gamma}$ now yields that $d\tilde{D}(x_1)/dx_1$ and $y_1(x_1)$ are identical functions of x_1, which implies

$$\tilde{\Gamma}(x_1')-\tilde{\Gamma}(x_1)=\int_{x_1}^{x_1'}[y_1(x)-H_1-Gx]dx \tag{3.2}$$

for $\{x_1,x_1'\}$ solutions of (2.12).

As a consequence of the equal-areas rule, if the curve $y_1(x_1)$ and (2.12) can intersect three times for a given G [slope of (2.12)], there will be a phase transition for some H_1 for which the enclosed areas become equal, whereas if there is only one intersection, the transition does not exist. Hence the condition for a first-order transition is that G exceeds the slope of $y_1(x_1)$ at its point of minimum slope, that is, its point of inflection.

Numerically determining the minimum slope of $y_1(x_1)$ for chosen values of Ω enables us to plot Fig. 1, the phase diagram in the $(G,r_1/\xi)$ plane. The critical line separates a one-phase region from a two-phase region of adsorption phase transitions. Note that for $1\le G\le 1.17$ the surface transitions ($r_1\gtrsim\xi$) and the point transitions ($r_1\lesssim\xi$) are separated by a one-phase region, whereas they are joined for $G>1.17$. In the limit $r_1/\xi\to 0$ the critical value of G approaches 1.

Analogous results for cylinders are shown in Fig. 2. Surface and line transitions are separate for $0\le G\le 0.33$ and are joined for $G>0.33$. For $r_1/\xi\to 0$, the critical value of G approaches 0.

For comparison, Fig. 3 displays the corresponding phase diagram for planar substrates, known since the global analysis of Nakanishi and Fisher.[3] Note the region of critical wetting (second-order phase transitions) which is absent for the curved substrates that we study. Also note that, as we move away from the origin along the critical lines in Figs. 1 and 2, we must recover, for $r_1\to\infty$, the slopes of the straight critical lines of Fig. 3. For $T>T_c$, this trend is clearly visible in the figures, but for $T<T_c$, the approach is much slower.

IV. ANALYTIC RESULTS FOR $T<T_c$

We now show that for *weakly varying profiles* (small $x+1$) it is possible to obtain an analytic approximation to the critical line. Note that all profiles are monotonic for $1\le\rho<\infty$, and consequently the profiles are weakly varying provided $x_1\approx -1$. Results are first derived for a spherical substrate and then an analogous derivation is outlined for a cylindrical substrate.

We first write (2.10) in the form

$$\ddot{x}+2\frac{\dot{x}}{\rho}-2\Omega(x+1)+P=0 \ , \tag{4.1}$$

where

$$P=\Omega(x+1)^2[3-(x+1)] \tag{4.2}$$

is considered to be a small perturbation. Defining

$$u=(2\Omega)^{1/2}, \quad t=u\rho, \quad w(t)=x(\rho)+1 \ , \tag{4.3}$$

Eq. (4.1) becomes

$$\ddot{w}+2\frac{\dot{w}}{t}-w+\frac{\epsilon}{2}w^2(3-w)=0 \ , \tag{4.4}$$

where ϵ is introduced to order the terms in the perturbation expansion and is put to 1 at the end of the calculation.

Assuming a solution of the form

$$w(t)=w_0(t)+\epsilon w_1(t)+\cdots \tag{4.5}$$

leads to a zeroth-order differential equation

$$\ddot{w}_0+2\frac{\dot{w}_0}{t}-w_0=0 \tag{4.6}$$

and a first-order $[O(\epsilon)]$ equation

$$\ddot{w}_1+2\frac{\dot{w}_1}{t}-w_1=-\tfrac{1}{2}w_0^2(3-w_0) \ , \tag{4.7}$$

which must be solved according to the boundary conditions

$$w_0(t=u)=1+x_1 \ , \tag{4.8a}$$

$$w_j(t=u)=0, \quad j\ge 1 \ , \tag{4.8b}$$

$$\lim_{t\to\infty} w_j(t)=0, \quad j\ge 0 \ . \tag{4.8c}$$

From (4.6) and (4.8) the zeroth-order solution is

$$w_0(t)=u(1+x_1)\frac{e^{(u-t)}}{t} \ . \tag{4.9}$$

The first-order solution can be found using the method of variation of parameters

$$w_1(t)=a(t)v_1(t)+b(t)v_2(t) \ , \tag{4.10}$$

where

$$v_1(t)=e^{-t}/t, \quad v_2(t)=e^t/t \tag{4.11}$$

are the solutions of the homogeneous equation, and

$$a(t)=\int_u^t dt'\frac{t'^2}{4}v_2(t')w_0^2(t')[3-w_0(t')]+a(u) \ , \tag{4.12}$$

$$b(t)=\int_t^\infty dt'\frac{t'^2}{4}v_1(t')w_0^2(t')[3-w_0(t')] \ , \tag{4.13}$$

where $a(u)$ is determined by the boundary conditions (4.8b).

From (2.11a), (4.3), (4.5), and (4.9)–(4.13) the curve of initial values is given to first order by

$$y_1(x_1)=(1+u)(1+x_1)-\tfrac{3}{2}u^2e^{3u}E_1(3u)(1+x_1)^2 +\tfrac{1}{2}u^2e^{4u}E_2(4u)(1+x_1)^3 , \quad (4.14)$$

where

$$E_n(x)=\int_1^\infty \frac{e^{-xs}}{s^n}ds .$$

Function (4.14) has a point of inflection at

$$\tilde{x}_1=-1+e^{-u}E_1(3u)/E_2(4u) , \quad (4.15)$$

which immediately gives the first-order approximation to the critical line

$$G\approx 1+u-\tfrac{3}{2}u^2e^{2u}E_1^2(3u)/E_2(4u) . \quad (4.16)$$

For small u this reduces to

$$G\sim 1+u-\tfrac{3}{2}u^2[\gamma_E+\ln(3u)]^2 , \quad (4.17)$$

where γ_E is Euler's constant.

Equation (4.16) agrees with the numerical results for the critical line to better than 1% for $r_1/\xi<0.1$. The position of the point of inflection $\tilde{x}_1$ is, however, given less accurately (an error of $\approx 10\%$ at $r_1/\xi\approx 0.1$). This has little effect on the critical value of G because $y_1(x_1)$ becomes a straight line ($y_1=x_1+1$) as $r_1/\xi\to 0$.

A similar calculation can be used to obtain the critical line for cylinders. Writing (2.15) as

$$\ddot{x}+\frac{\dot{x}}{\rho}-2\Omega(x+1)+P=0 \quad (4.18)$$

and calculating to first order in the nonlinear perturbation P, we obtain

$$y_1(x_1)=u[K_1(u)/K_0(u)](x_1+1) -\tfrac{3}{2}[\Lambda_3(u)/K_0^3(u)](x_1+1)^2 +\tfrac{1}{2}[\Lambda_4(u)/K_0^4(u)](x_1+1)^3 , \quad (4.19)$$

where K_0 and K_1 are modified Bessel functions and

$$\Lambda_n(u)=\int_u^\infty xK_0^n(x)dx . \quad (4.20)$$

Hence, to first order

$$G=uK_1(u)/K_0(u)-\tfrac{3}{2}\Lambda_3^2(u)/[\Lambda_4(u)K_0^2(u)] . \quad (4.21)$$

For small u this reduces to

$$G\approx -[\gamma_E+\ln(u/2)]^{-1} . \quad (4.22)$$

Equation (4.21) agrees with the numerical results for the critical line to better than 10% for $r_1/\xi<0.01$. For the ordinate $\tilde{y}_1$ of the inflection point we find numerically, for $T\to T_c$, $\tilde{y}_1\approx 0.622$, whereas the first-order approximation (4.19) gives $\tilde{y}_1\approx 0.557[=\Lambda_3(0)/\Lambda_4(0)]$.

Note that (4.19) may be expected to be an accurate approximation as long as the magnitude of consecutive terms decreases rapidly enough. Generally, x_1+1 must be small for this, but for $u\to 0$ it suffices that $(\ln u)^{-1}(x_1+1)$ be small. One can thus expect better accuracy in this limit. However, the inflection point coordinate $\tilde{x}_1$ lies at $(\ln u)^{-1}(\tilde{x}_1+1)\approx 1$, so that for $u\to 0$ we should not expect (4.19) to yield the exact location of the critical line. Indeed, G, as given by (4.21), becomes increasingly accurate as $u\to 0$, but $\tilde{y}_1$ approaches a constant which differs $\approx 10\%$ from the correct one. We shall see later that the values of H_1 along the critical line are also given quite accurately by (4.21), as $u\to 0$ (see Sec. VII).

Next we would like to present exact inequalities which provide a useful bound for the location of the critical line. From (3.1) follows the trivial bound

$$\frac{y_1^2}{2}\geq\frac{\Omega}{4}(x_1^2-1)^2 \quad (4.23)$$

since $y(x)\geq 0$ for $x_1>-1$ and $y(x)\leq 0$ for $x_1<-1$. Furthermore, $y_1(x_1)$ is concave in $x_1=-1$ because of (4.19). Consequently, the slope of $y_1(x_1)$ is not minimal in $x_1=-1$ and we obtain a *sufficient* condition for the existence of a first-order phase transition by requiring that G exceed the slope of $y_1(x_1)$ in $x_1=-1$. Thus, the phase transition must occur for

$$G\geq uK_1(u)/K_0(u) , \quad (4.24)$$

which reduces to

$$G\geq -[\gamma_E+\ln(u/2)]^{-1} \quad (4.25)$$

for $u\to 0$. This provides an analytic argument for the existence of the line transitions ($r_1\lesssim\xi$) for all $G>0$.

Note that a similar argument holds in the case of the spherical substrates. For spheres, the phase transition must occur for

$$G\geq 1+u . \quad (4.26)$$

Finally we would like to draw attention to another useful analytic approximation, which is an expansion in Ω, thus valid for T close to T_c or, equivalently, large curvature. Such an expansion, however, amounts to singular perturbation theory,[13] because already in zeroth order (for the cylinders) and in first order (for the spheres) it is not possible to satisfy the boundary condition (2.13). The expansion is only useful for sufficiently small $t=(2\Omega)^{1/2}\rho$. For large t, on the other hand, one can successfully use the zeroth-order result (4.9) of the expansion in $x+1$. The two expansions can be matched at arbitrary $t\approx 1$. In the Appendix we give the expansions in Ω to (and including) first order.

V. EXACT RESULTS FOR $T>T_c$

For temperatures above the bulk critical temperature the symmetry of the problem requires that the point of inflection of the curve of initial conditions $y_1(x_1)$ is at $x_1=0$. Hence it is sufficient to linearize the equation of motion in x, to obtain the slope at the origin, and hence the critical G as a function of r_1/ξ. Furthermore, the phase transitions occur for $h_1=0$ by symmetry.

For $T>T_c$ the bulk free-energy density (2.2) is

$$f(m(r))=cm^2/(2\xi^2)+m^4 , \tag{5.1}$$

and hence the free-energy functional for a spherical substrate (2.1) written in the reduced units

$$\rho=r/r_1 \quad x=x(\rho)=m(r)2\xi/c^{1/2} \tag{5.2}$$

becomes

$$\Gamma[x]=\int_1^\infty d\rho\rho^2\left[\frac{1}{2}\left[\frac{dx}{d\rho}\right]^2+\frac{\Omega}{4}(2x^2+x^4)\right] -H_1x_1-Gx_1^2/2 , \tag{5.3}$$

where $H_1=r_1h_1 2\xi/c^{3/2}$, $G=r_1g/c$, and $\Omega=(r_1/\xi)^2$. This leads to an Euler-Lagrange equation

$$\ddot{x}+2\frac{\dot{x}}{\rho}=\Omega x(x^2+1) . \tag{5.4}$$

Linearizing (5.4) about $x=0$ and solving it subject to the boundary conditions

$$y_1=H_1+Gx_1 , \tag{5.5a}$$

$$\lim_{\rho\to\infty} x(\rho)=0 \tag{5.5b}$$

[cf. (2.12) and (2.13)] gives

$$y=-dx/d\rho=\Omega^{1/2}x_1\exp[\Omega^{1/2}(1-\rho)]/\rho +x_1\exp[\Omega^{1/2}(1-\rho)]/\rho^2+O(x_1^3) . \tag{5.6}$$

Hence the critical line is given by

$$G=dy_1/dx_1|_{x_1=0}=1+\Omega^{1/2}, \quad H_1=0 . \tag{5.7}$$

This result is shown in Fig. 1 (bottom part). It is exact for all $T>T_c$ because the point of inflection of $y_1(x_1)$ is at $x_1=0$. The result provided a useful check of the numerical algorithms used to obtain the critical line for $T<T_c$.

Results for cylinders for $T>T_c$ are obtained in an entirely analogous manner. The equation of motion

$$\ddot{x}+\frac{\dot{x}}{\rho}=\Omega x(x^2+1) \tag{5.8}$$

is linearized and solved to give

$$y=-dx/d\rho=\Omega^{1/2}x_1K_1(\Omega^{1/2}\rho)/K_0(\Omega^{1/2})+O(x_1^3) . \tag{5.9}$$

Hence

$$G=dy_1/dx_1|_{x_1=0}=\Omega^{1/2}K_1(\Omega^{1/2})/K_0(\Omega^{1/2}), \quad H_1=0 , \tag{5.10}$$

defines the critical line. This is shown in Fig. 2 (bottom part).

VI. EXACT RESULTS FOR $T=T_c$

We now discuss, by obtaining bounds on the behavior of $y_1(x_1)$ at the origin, the adsorption phase transitions at T_c. We find a critical value $G=0$ for cylinders and $G=1$ for spheres, as expected from the results for temperatures above and below T_c.

A. Spheres

For spheres at T_c the equation of motion becomes

$$\ddot{x}+2\frac{\dot{x}}{\rho}=\omega x^3 , \tag{6.1}$$

where $x=x(\rho)=m(r)$ and $\omega=4r_1^2/c$. The nonlinear force x^3 prevents an expansion in x. Integrating (6.1) subject to the boundary conditions (5.5) gives

$$\frac{y_1^2}{2}-\frac{\omega}{4}x_1^4=2\int_0^{x_1}\frac{y}{\rho}dx . \tag{6.2}$$

1. *Upper bound*

We consider a particle satisfying the equation of motion

$$\ddot{\tilde{x}}+2\frac{\dot{\tilde{x}}}{\tilde{\rho}}=0 . \tag{6.3}$$

This should be compared to (6.1). It includes friction but no force term. The solution to (6.3) which obeys the initial conditions $\tilde{x}_1=x_1$ and $\tilde{y}_1=y_1$ is

$$\tilde{y}=y_1/\tilde{\rho}^2 , \tag{6.4a}$$

$$\tilde{x}=x_1-y_1+y_1/\tilde{\rho} . \tag{6.4b}$$

Note that, for all $\rho\geq 1$,

$$|\tilde{y}(\rho)|\geq|y(\rho)| , \tag{6.5}$$

which follows directly from (6.1), (6.3), and $\tilde{y}_1=y_1$. Then, clearly,

$$|\tilde{y}(x)|\geq|y(x)| \text{ for } |x|\leq|x_1| . \tag{6.6}$$

Consequently,

$$\tilde{\rho}(x)\leq\rho(x) . \tag{6.7}$$

Using these inequalities and (6.4) in (6.2) gives

$$y_1^2(x_1/y_1-1)^4\leq\tfrac{1}{2}\omega x_1^4 . \tag{6.8}$$

2. *Lower bound*

Note that in (6.4b) $\tilde{x}(\tilde{\rho}=\infty)=x_1-y_1$. Since we have (6.6) we must have

$$|y_1|\geq|x_1| . \tag{6.9}$$

From (6.8) and (6.9) it follows that the slope of $y_1(x_1)$ must be 1 for $x_1\to 0$, and hence that the critical point for the phase transitions is at $G=1$.

B. Cylinders

For cylinders at T_c, the equation of motion becomes

$$\ddot{x}+\frac{\dot{x}}{\rho}=\omega x^3 . \tag{6.10}$$

Integrating this subject to the boundary conditions (5.5) gives

$$\frac{y_1^2}{2}-\frac{\omega}{4}x_1^4=\int_0^{x_1}\frac{y}{\rho}dx \ . \tag{6.11}$$

1. Upper bound

Proceeding as for spheres we solve the problem without force term

$$\ddot{\tilde{x}}+\frac{\dot{\tilde{x}}}{\tilde{\rho}}=0 \ , \tag{6.12}$$

subject to the initial conditions $\tilde{x}_1=x_1$, and $\tilde{y}_1=y_1$, to give

$$\tilde{y}=y_1/\tilde{\rho} \ , \tag{6.13a}$$

$$\tilde{x}=x_1-y_1\ln\tilde{\rho} \ . \tag{6.13b}$$

Using the inequalities (6.6) and (6.7), which are equally valid here, and (6.13) in (6.11) gives

$$y_1^2\le\tfrac{1}{2}\omega x_1^4 e^{2x_1/y_1} \ . \tag{6.14}$$

2. Lower bound

A lower bound

$$y_1^2\ge\tfrac{1}{2}\omega x_1^4 \tag{6.15}$$

follows immediately from noting that the right-hand side of (6.11) must be non-negative. Now (6.14) and (6.15) imply that the slope of $y_1(x_1)$ tends to zero as $x_1\to 0$ and hence that the critical point for the phase transitions is at $G=0$.

Numerical computations indicate that $y_1(x_1)$ is well approximated by

$$y_1(x_1)\approx -x_1/\ln|x_1|, \quad x_1\to 0 \ , \tag{6.16}$$

a result which satisfies the bounds (6.14) and (6.15).

VII. SURFACE FIELD ALONG THE CRITICAL LINE NEAR T_c

In this section we examine how the surface field h_1 varies as a function of r_1/ξ for $r_1/\xi\to 0$ along the critical line. For $T\ge T_c$ we trivially have $h_1=0$ at the phase transitions. For $T<T_c$, we first use the analytic approximations (4.14) and (4.19) for $y_1(x_1)$. Let $\bar{x}_1$ and $\bar{y}_1$ denote the coordinates of the inflection point of $y_1(x_1)$. The surface field at the critical transition is then given by the intercept of the tangent at $(\bar{x}_1,\bar{y}_1)$, or

$$H_1=\bar{y}_1-G\bar{x}_1 \ . \tag{7.1}$$

We obtain

$$H_1\approx 1+u+\tfrac{1}{2}u^2e^u E_1^3(3u)/E_2^2(4u) -\tfrac{3}{2}u^2e^{2u}E_1^2(3u)/E_2(4u) \ , \tag{7.2}$$

for $u=(2\Omega)^{1/2}\to 0$, for spheres and

$$H_1\approx[uK_1(u)+\tfrac{1}{2}\Lambda_3^3(u)/\Lambda_4^2(u)]/K_0(u) -\tfrac{3}{2}[\Lambda_3^2(u)/\Lambda_4(u)]/K_0^2(u) \ , \tag{7.3}$$

for $u\to 0$, for cylinders.

The agreement of these asymptotic results with the numerical computations is excellent. We therefore propose that the following mean-field critical exponents describe the surface field along the critical line, as $T\to T_c^-$ ($r_1/\xi\to 0$, with r_1 fixed):

$$h_1\propto(T_c-T)^{1/2} \text{ for spheres} \ , \tag{7.4}$$

$$h_1\propto -(T_c-T)^{1/2}/\ln(T_c-T) \text{ for cylinders} \ . \tag{7.5}$$

This is to be compared with the corresponding behavior for the planar substrate,

$$h_1\propto T_c-T \tag{7.6}$$

along the tricritical line.

VIII. PREWETTING

The phenomenon of prewetting in a flat geometry is well understood theoretically,[1-3,5] but has eluded experimental detection so far.[14,15] The prewetting phase transition is the extension of a first-order wetting phase transition into the bulk one-phase region (off coexistence). For example, when a flat substrate preferentially adsorbs the liquid phase ($h_1>0$) and the adsorbate is in the vapor phase because of the presence of a bulk field $h<0$, there can be a prewetting transition between a thin and a thick wetting layer. Clearly, the wetting layer cannot be macroscopically thick because the liquid is not stable in bulk. Thus we see that the bulk field imposes a finite layer thickness. We have already seen that curvature also imposes a finite layer thickness, even at bulk coexistence. In this section we are dealing with adsorption phase transitions in the presence of both curvature and a bulk field.

In the presence of a bulk field h, the bulk free-energy density takes the form [cf. (2.2)]

$$f(m)=a_0-hm+2(T-T_c)m^2+m^4 \ , \tag{8.1}$$

where a_0 is such that $\min[f(m)]=0$. Prewetting and prewetting criticality have been studied systematically in a flat geometry.[3] We restrict ourselves to mentioning one particular result in the limit $h\to 0^-$, at fixed temperature $T<T_c$. For a flat substrate, the curve of initial conditions $\tilde{y}_1(x_1)$ satisfies, with $m_b^2=T_c-T=m_b^2$ ($h=0$),

$$\frac{\tilde{y}_1^2}{2}\sim(x_1^2-1)^2m_b^2/c-h(x_1+1)m_b^{-1}/c+O(h^2) \ , \tag{8.2}$$

where a surface free-energy functional analogous to (2.1) is assumed for a profile $x(z)=m(z)/m_b$, for $1\le z<\infty$ and $\tilde{y}(z)=-dx(z)/dz$. The reason for mentioning (8.2) will become clear when we discuss (Sec. XI) the curve $y_1(x_1)$ for curved substrates in the limit of small curvature.

For spherical and cylindrical substrates, the introduction of a bulk field h leads to the differential equation for the profile $x(\rho)$,

$$\ddot{x}+p\frac{\dot{x}}{\rho}=\Omega x(x^2\pm 1)-H \ , \tag{8.3}$$

where, from here on, $p=1$ for cylinders and $p=2$ for spheres. The $+$ sign refers to $T>T_c$ and the $-$ sign to $T<T_c$, and, with $m_b=m_b\ (h=0)$,

$$x(\rho)=m(r)/m_b \ , \tag{8.4}$$

$$H=2\xi(h=0)r_1^2 h/c^{3/2} \tag{8.5}$$

$$=r_1^2 h/(cm_b), \text{ for } T<T_c \ . \tag{8.6}$$

The definition of Ω, and the boundary conditions are the same as before, except that now $\lim_{\rho\to\infty}x(\rho)=x_\infty$, where x_∞ solves

$$x_\infty^3 \pm x_\infty - 2h\xi^3/c^{3/2}=0 \ . \tag{8.7}$$

Clearly, for $T<T_c$ ($-$ sign) that solution must be considered which approaches -1 as $h\to 0$ at fixed T. For small $h\xi^3$, we obtain

$$x_\infty \sim \begin{cases} -1+h\xi^3/c^{3/2}, & T<T_c \quad (8.8a) \\ 2h\xi^3/c^{3/2}, & T>T_c. \quad (8.8b) \end{cases}$$

In the following we derive analytic approximations to the critical surfaces which bound the two-phase regions of adsorption phase transitions. These critical surfaces are the extensions of the critical lines (see Figs. 1 and 2) into the bulk one-phase region ($h\neq 0$).

Let $w(\tau)=x(\rho)-x_\infty$ and $\tau=\alpha_\pm\rho$, where

$$\alpha_\pm=[(3x_\infty^2\pm 1)\Omega]^{1/2} \ . \tag{8.9}$$

The differential equations then become

$$\ddot{w}+p\frac{\dot{w}}{\tau}-w=(3x_\infty w^2+w^3)/(3x_\infty^2\pm 1) \ . \tag{8.10}$$

Performing a perturbation expansion as in Sec. IV, we obtain an expansion of the initial condition curve $y_1(x_1)$ in powers of x_1-x_∞. We find, for spheres,

$$y_1(x_1)\approx(1+\alpha_\pm)(x_1-x_\infty) + \frac{3x_\infty}{(3x_\infty^2\pm 1)}\alpha_\pm^2 e^{3\alpha_\pm}E_1(3\alpha_\pm)(x_1-x_\infty)^2 + \frac{\alpha_\pm^2}{(3x_\infty^2\pm 1)}e^{4\alpha_\pm}E_2(4\alpha_\pm)(x_1-x_\infty)^3 \tag{8.11}$$

and, for cylinders,

$$y_1(x_1)\approx\alpha_\pm[K_1(\alpha_\pm)/K_0(\alpha_\pm)](x_1-x_\infty) + \frac{3x_\infty}{(3x_\infty^2\pm 1)}[\Lambda_3(\alpha_\pm)/K_0^3(\alpha_\pm)](x_1-x_\infty)^2 + \frac{1}{(3x_\infty^2\pm 1)}[\Lambda_4(\alpha_\pm)/K_0^4(\alpha_\pm)](x_1-x_\infty)^3 \ . \tag{8.12}$$

From this we calculate the following approximations to the critical values of G and H_1. For spheres,

$$G\approx 1+\alpha_\pm-\frac{3x_\infty^2}{(3x_\infty^2\pm 1)}\alpha_\pm^2 e^{2\alpha_\pm}E_1^2(3\alpha_\pm)/E_2(4\alpha_\pm) \ , \tag{8.13}$$

$$H_1\approx-(1+\alpha_\pm)x_\infty-\frac{x_\infty^3\alpha_\pm^2}{(3x_\infty^2\pm 1)}e^{\alpha_\pm}E_1^3(3\alpha_\pm)/E_2^2(4\alpha_\pm) + \frac{3x_\infty^3}{(3x_\infty^2\pm 1)}\alpha_\pm^2 e^{2\alpha_\pm}E_1^2(3\alpha_\pm)/E_2(4\alpha_\pm) \ . \tag{8.14}$$

For cylinders,

$$G\approx\alpha_\pm K_1(\alpha_\pm)/K_0(\alpha_\pm) - \frac{3x_\infty^2}{(3x_\infty^2\pm 1)}\Lambda_3^2(\alpha_\pm)/[\Lambda_4(\alpha_\pm)K_0^2(\alpha_\pm)] \ , \tag{8.15}$$

$$H_1\approx-\alpha_\pm K_1(\alpha_\pm)x_\infty/K_0(\alpha_\pm) - \frac{x_\infty^3}{(3x_\infty^2\pm 1)}\Lambda_3^3(\alpha_\pm)/[\Lambda_4^2(\alpha_\pm)K_0(\alpha_\pm)] + \frac{3x_\infty^3}{(3x_\infty^2\pm 1)}\Lambda_3^2(\alpha_\pm)/[\Lambda_4(\alpha_\pm)K_0^2(\alpha_\pm)] \ . \tag{8.16}$$

Note that (8.13) reduces to (4.16) and (5.7), (8.14) reduces to (7.2), (8.15) reduces to (4.21) and (5.10), and (8.16) reduces to (7.3), for $h\to 0$.

Furthermore, we can obtain exact inequalities for the occurrence of adsorption phase transitions. The second derivative of $y_1(x_1)$ at $x_1=x_\infty$ is proportional to x_∞ [see (8.11) and (8.12)]. Consequently, the inflection point of $y_1(x_1)$ is not at x_∞, unless $T>T_c$ *and* $h=0$. Thus we obtain the following lower bounds on G for the occurrence of the phase transitions. For spheres,

$$G\geq 1+\alpha_\pm \ , \tag{8.17}$$

and, for cylinders,

$$G\geq\alpha_\pm K_1(\alpha_\pm)/K_0(\alpha_\pm) \ . \tag{8.18}$$

For $h\to 0$, (8.17) reduces to (4.26) for $T<T_c$ and to the exact result (5.7) for $T>T_c$, and (8.18) reduces to (4.24) for $T<T_c$ and to the exact result (5.10) for $T>T_c$.

IX. WETTING LAYER THICKNESSES

In this section we study the wetting layer thicknesses in two different limits: the planar limit ($r_1\to\infty$, ξ fixed) and the limit of high curvature or criticality ($r_1/\xi\to 0$). In the planar limit the wetting layer is physically well identifiable. We argue that its thickness R is proportional to $\xi\ln(r_1/\xi)$, a result which, for spherical substrates, was already obtained in earlier work where use was made of the double-parabola approximation.[8] In the opposite limit of high curvature, the concept of a wetting layer is much less clear. It is more appropriate to speak of an order-parameter profile which varies significantly over a "thickness" R before reaching its limiting value in bulk. We argue that $R\propto\xi$. Our results are based on approximate analytical arguments.

In the planar limit a typical wetting layer profile is

shown in Fig. 4 ($r_1/\xi=10^4$). We have $\xi \ll r_1 < \infty$. The profile consists of a rapid initial decay towards the bulk "liquid" density, followed by a region of nearly constant density, the wetting layer. Finally, the profile decays via a liquid-vapor interfacial structure into the bulk vapor phase.

Define $x(r)\equiv m(r)/m_b$, and $\dot{x}=dx/dr$. The thickness l of the region of rapid initial decay is well approximated by

$$l=\int_{r_1}^{r_1+l} dr=-\int_{\hat{x}}^{x_1}(1/\dot{x})dx \ , \tag{9.1}$$

where $x_1=x(r_1)$ and $\hat{x}$ is a suitable value slightly greater than 1 (for example, $\hat{x}=1.1$). We then have by virtue of an inequality similar to (4.23)

$$l \lesssim (\xi/2^{1/2})\ln\{(x_1-1)(\hat{x}_1+1)/[(x_1+1)(\hat{x}_1-1)]\} \ . \tag{9.2}$$

This signifies that l is of order ξ. The same conclusion applies to the thickness of the liquid-vapor interfacial structure which bounds the wetting layer on the other side.

To study the profile after the initial decay, we start from the differential equation

$$\ddot{x}+p\frac{\dot{x}}{r}=\xi^{-2}x(x^2-1) \ . \tag{9.3}$$

We perform an expansion in $1/r_1$. This leads to

$$x(r)=x^{(0)}(r)+x^{(1)}(r)/r_1+\cdots \ , \tag{9.4}$$

$$\ddot{x}^{(0)}=\xi^{-2}x^{(0)}(x^{(0)^2}-1) \ , \tag{9.5}$$

$$\ddot{x}^{(1)}+p\dot{x}^{(0)}=\xi^{-2}(3x^{(0)^2}-1)x^{(1)} \ . \tag{9.6}$$

The initial conditions are

$$x^{(0)}(r_1+l)=\hat{x}, \quad x^{(1)}(r_1+l)=0 \ . \tag{9.7}$$

Since $\hat{x}>1$, we have

$$x^{(0)}(\infty)=1 \ . \tag{9.8}$$

For $\hat{x}\approx 1$ we have $x^{(0)}(r)\approx 1$ for $r_1+l\le r<\infty$, so that (9.6) can be approximated by

$$\ddot{x}^{(1)}+p\dot{x}^{(0)}=2\xi^{-2}x^{(1)} \ . \tag{9.9}$$

Note that (9.9) would also result from linearizing (9.3) in $x-1$, before expanding in $1/r_1$. However, (9.5) would then be affected as well. In the present scheme, (9.5) is exact in the planar limit.

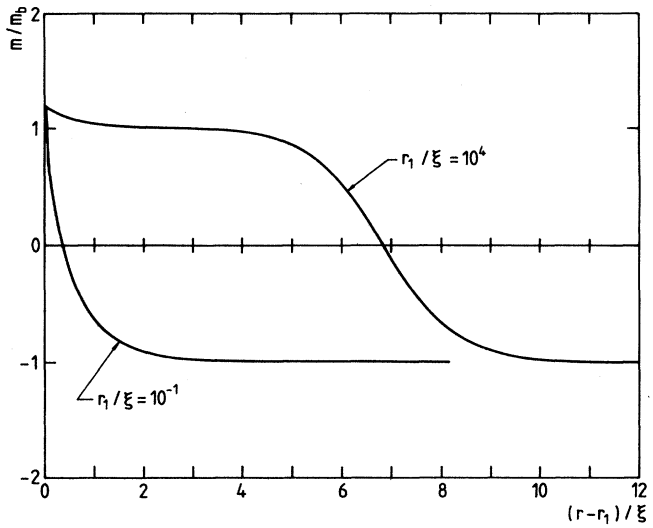

FIG. 4. Profiles of reduced order parameter $m(r)/m_b$ vs reduced radial distance from the cylindrical substrate $(r-r_1)/\xi$. Two cases are shown. For $r_1/\xi=10^4$ the substrate curvature is small and the adsorbate is away from criticality. The profile has a pronounced "shoulder" corresponding to the wetting layer with thickness of order $\xi\ln(r_1/\xi)$. For $r_1/\xi=10^{-1}$ the substrate is strongly curved and the adsorbate is close to criticality. The profile decays in a featureless fashion over a distance of order ξ. In both cases the boundary conditions are chosen to be $m(r_1)/m_b=1.2$ and $m(\infty)/m_b=-1$.

The solution to (9.5) is given by

$$x^{(0)}(r)=\coth(\alpha z/2+\phi) \ , \tag{9.10}$$

with $z=r-r_1-l$, $\alpha=2^{1/2}/\xi$, and $\phi=\coth^{-1}(\hat{x})$. The solution to (9.9) is given by

$$(2\alpha/p)x^{(1)}(r)=e^{\alpha z}(A-\int_0^z e^{-\alpha z'}\dot{x}^{(0)}(z')dz') +e^{-\alpha z}(-A+\int_0^z e^{\alpha z'}\dot{x}^{(0)}(z')dz') \ . \tag{9.11}$$

The constant of integration A can be determined, in principle, by constructing a complementary approximation for $-1<x<1$ and matching the two approximations.

The integrals in (9.11) are worked out to give

$$(\alpha/p)x^{(1)}(r)=A\sinh\alpha z+\hat{x}\sinh\alpha z+\cosh\alpha z-1-2\cosh(\alpha z+2\phi)\ln[(e^{\alpha z+2\phi}-1)/(e^{2\phi}-1)]+e^{\alpha z+2\phi}\alpha z \ . \tag{9.12}$$

For large αz this leads to, using (9.4),

$$x(r)\sim x^{(0)}(r)-B(A,\hat{x})(p\xi/r_1)\exp[2^{1/2}(r-r_1-l)/\xi] \ . \tag{9.13}$$

Now the use of the expansion is clear. The zeroth-order profile satisfies $x^{(0)}(r)\to 1$, for $r\to\infty$. The first-order profile closely follows $x^{(0)}(r)$ until the correction term becomes of order 1. This takes place for

$$r-r_1-l\propto\xi\ln(r_1/p\xi) \ . \tag{9.14}$$

This signifies that the wetting layer terminates when (9.14) is satisfied. Note that the amplitude B is not ex-

plicitly calculated. We expect B to be finite for $x_1 > 1$, that is, as long as the wetting layer is clearly identifiable.

We conclude that, for both spheres and cylinders, the wetting layer thickness for $r_1 \gg \xi$ is given by (9.14). Note that the layer thickness grows extremely slowly with increasing r_1. For example, in this Landau theory with short-range substrate-adsorbate forces, the thickness of the wetting layer on a sphere with the radius of the earth is only ≈ 100 correlation lengths.

Numerical computations appear to support (9.14). For example, for cylinders, we obtain for $r_1/\xi \to \infty$,

$$\bar{r} - r_1 \approx 0.69\xi \ln(r_1/\xi) , \tag{9.15}$$

where $\bar{r}$ is defined by $x(\bar{r}) = 0$, and we have taken the initial condition $x(r_1) = 1.1$, and, of course, $x(\infty) = -1$.

In the opposite limit, $r_1 \ll \xi < \infty$, a typical profile is displayed in Fig. 4 ($r_1/\xi = 10^{-1}$). The thickness R of the adsorbed layer can be defined as the radial distance beyond which the deviations of the order parameter from its asymptotic bulk value are exponentially small. We readily find R by inspection of the expansions in r_1/ξ (see the appendix).

For spheres, it follows immediately that $R \propto \xi$, because the solution for small r, (A3)–(A4), can be matched to the solution for large r, precisely when $r/\xi \approx 1$. Furthermore, (A8) implies that the profile has only exponentially small deviations from its bulk value -1 as soon as $r > \xi$.

For cylinders, the matching needs to be done for r slightly smaller than ξ, because of the presence of the logarithmic corrections in (A16). From (A17) it is clear that exponentially small deviations from the bulk order parameter again require $r > \xi$.

We conclude that $R \propto \xi$ for both spheres and cylinders, in the regime $r_1 \ll \xi$. Consequently, the wetting-layer thickness can be arbitrarily large relative to the substrate radius.

X. FINITE-SIZE ROUNDING OF FIRST-ORDER PHASE TRANSITIONS

The substrate-adsorbate systems we are studying are three dimensional ($d = 3$). In the thermodynamic limit the substrates remain finite in two (cylinders) or three (spheres) dimensions of space. Due to finite-size effects the adsorption phase transitions will be rounded, they will not be sharp first-order phase transitions as they are for a (flat) two-dimensional substrate. Gelfand and Lipowsky already made this point in the context of wetting on cylinders and spheres,[9] and gave both qualitative and quantitative estimates of the importance of these effects in the regime $r_1 \gg \xi$. We discuss also the regime $r_1 < \xi$. Furthermore, we consider not only $T < T_c$, but $T > T_c$ and $T = T_c$ as well.

Finite-size rounding of first-order phase transitions has been studied in great detail and in a rather general context by Privman and Fisher.[16] We attempt to apply their formalism and basic results to our case. Basically, they have considered bulk phase transitions inside a finite volume, whereas we consider surface phase transitions on the outside of a finite volume.

For a subset of adsorption phase transitions, namely the *prewetting* transitions (off coexistence, $h \neq 0$) and the *pure surface* transitions ($T > T_c$, $g > 0$, $h = 0$), there is a clear universality-class argument which explains why these transitions are sharp for flat substrates, but rounded for cylinders and spheres. Nakanishi and Fisher[3] showed that the prewetting transitions are smoothly connected to the pure surface transitions, in the phase diagram topology. Therefore, both types of phenomena are essentially the same. In particular, prewetting criticality and pure surface criticality are expected to be in the same universality class, namely, in our case, that of the Ising model with the dimensionality of the substrate, d_s. For a flat substrate, $d_s = 2$, so that the phase transition can occur for $T > 0$. For cylinders ($d_s = 1$) and spheres ($d_s = 0$), sharp phase transitions cannot occur for $T > 0$. The phase transitions must be rounded.

In our opinion, one cannot apply the same universality-class argument for the first-order *wetting* transitions ($T < T_c$, $h = 0$), because wetting criticality and prewetting criticality are in different universality classes.[3] Moreover, genuine wetting phase transitions (albeit continuous ones) can take place on substrates with $d_s = 1$, for $T > 0$.[17] We prefer to argue that the wetting transitions on cylinders and spheres must be rounded, not because of the reduced dimensionality of the substrate, but on the basis of the *geometry* of the substrate-adsorbate system. Firstly, the finite thickness of the wetting layer is clearly the result of the geometry of the emerging liquid-vapor interface. Secondly, because of the finite layer thickness on a cylinder, for example, there is the possibility of introducing kinklike fluctuations of the surface order parameter, along the cylinder axis. Such kink costs a finite energy but yields an entropy which diverges as the logarithm of the cylinder length. Thus, kinks are favorable and long-range surface order is destroyed for $T > 0$.

Following Privman and Fisher[16] we will proceed to make our considerations more quantitative. In general the rounding of the surface free energy γ is described by

$$\Delta\gamma \equiv \gamma(\delta h_1, T; r_1) - \gamma(0, T; \infty) \approx \frac{k_B T}{A_{\text{cor}}} , \tag{10.1}$$

where δh_1 is the surface field h_1 minus its value at the phase transition for $r_1 = \infty$. The "correlation area" A_{cor} is a measure of the substrate area occupied by a single domain of either of the two surface phases. Clearly, $A_{\text{cor}} \to \infty$ for $r_1 \to \infty$, reflecting the emergence of macroscopic surface phases with long-range order in this limit. In the following, r_1 is assumed to be much larger than microscopic lengths such as the molecular size.

A. Spherical substrates

The area available for domains is necessarily bounded by the area of the sphere, so that

$$\Delta\gamma \approx k_B T / r_1^2, \quad r_1 \to \infty . \tag{10.2}$$

Consequently, the finite-size rounding is "algebraically small" in the substrate radius. The bulk correlation

length ξ does not play a significant role. Indeed, Eq. (10.2) holds for $T \neq T_c$ and $T = T_c$. In the latter case, (10.2) describes the rounding of the *extraordinary transition* E ($g > 0$, see Fig. 3).

The surface correlation length $\xi^{(s)}$, however, plays an important role. For $r_1 = \infty$, $\xi^{(s)}$ diverges when the surface phase transition becomes critical. This is the case at *wetting criticality* ($T < T_c$), the *special transition* S ($T = T_c$), and *pure surface criticality* ($T > T_c$), all shown in Fig. 3. Clearly, the phase transitions will be wiped out by fluctuations in the regime $\xi^{(s)} > r_1$.

B. Cylindrical substrates

The area occupied by a domain can be arbitrarily large, in principle. The typical distance between domain walls which wind around the cylinder (and which are assumed responsible for breaking up long-range order) is the longitudinal correlation length $\xi_\parallel$. Therefore,

$$\Delta\gamma \approx \frac{k_B T}{r_1 \xi_\parallel}, \quad r_1 \to \infty \ . \tag{10.3}$$

In other words, $\xi_\parallel$ represents the mean separation (along the cylinder axis) between the kinklike fluctuations of the surface order parameter. $\xi_\parallel$ depends on three other lengths,

$$\xi_\parallel = \xi_\parallel(r_1, \xi, \xi^{(s)}) \ . \tag{10.4}$$

In general, $\xi_\parallel$ can be related to a domain-wall free energy Σ (per unit length of circumference) for which finite-size scaling predicts

$$\Sigma(r_1, \xi, \xi^{(s)}) = \xi^{(s)-1} X(r_1/\xi^{(s)}, \xi/\xi^{(s)}) \ . \tag{10.5}$$

The function $\xi_\parallel$ is well approximated by

$$\xi_\parallel \approx r_1 D(\xi/r_1, \xi^{(s)}/r_1) \exp[r_1 X(r_1/\xi^{(s)}, \xi/\xi^{(s)})/\xi^{(s)}] \ , \tag{10.6}$$

where D is a slowly varying function (e.g., algebraic) of its arguments (see, for example, Ref. 16).

In view of (10.5), the domain-wall free energy Σ vanishes as $\xi^{(s)-1}$ for $\xi^{(s)} \to \infty$. We will see that the finite-size rounding is always "exponentially small" in $r_1/\xi^{(s)}$. This means that if we are sufficiently far from the critical lines in the phase diagram for $r_1 = \infty$ (inside the two-phase regions, Fig. 3), so that $\xi^{(s)}$ is small, the rounding will be negligible for large r_1. Let us now see this in more detail.

Consider first the wetting transitions. We have $T < T_c$, $\xi^{(s)}$ finite, and $r_1 \to \infty$. Then we expect the scaling function X to diverge with r_1, because the wetting layer thickness diverges according to (9.14), and Σ approaches the product of the bulk interfacial tension σ (of a liquid-vapor interface) and the layer thickness. Explicitly, for $\xi^{(s)} \ll r_1$ and $\xi \ll r_1$,

$$\Sigma \approx \sigma \xi \ln(r_1/\xi), \quad r_1 \to \infty \ . \tag{10.7}$$

In other words, the kinklike fluctuation consists, for $r_1 \to \infty$, of a bulk interface standing perpendicular to the cylinder (on the outside). Therefore, the rounding is exponentially small in $r_1/\xi^{(s)}$, in view of Eqs. (10.5)–(10.7).

Secondly, consider the pure surface transitions. We have $T > T_c$, $\xi^{(s)}$ finite, and $r_1 \to \infty$. Then X is expected to approach a finite limit because the kinklike fluctuation penetrates only a distance of order ξ into the single-phase bulk. In other words, the order parameter profile $m(r)$ approaches the bulk order-parameter value exponentially fast over a length scale ξ. Thus, the rounding is exponentially small in $r_1/\xi^{(s)}$.

Thirdly, consider the extraordinary transition E. We have $T = T_c$ ($\xi = \infty$), $\xi^{(s)}$ finite ($g > 0$), and $r_1 \to \infty$. In this case it is not obvious whether X approaches a finite value or diverges. It is even possible that X is infinite for finite r_1. The latter possibility exists in view of the fact that the kinklike fluctuation decays algebraically into the critical bulk, instead of exponentially. This in turn is due to the algebraic decay of the order parameter profile $m(r)$, which obeys (6.10).[18] In any case, the rounding will be exponentially small in $r_1/\xi^{(s)}$ (finite X), or even smaller (divergent X).

In summary, for cylinders

$$\Delta\gamma \approx k_B T/[r_1^2 \exp(r_1/\xi^{(s)})], \quad r_1 \to \infty \ , \tag{10.8}$$

or possibly smaller.

Note that we emphasize the role of the surface correlation length $\xi^{(s)}$. Equations (10.2) and (10.8) imply that we can, in practice, neglect the finite-size rounding, *regardless of the magnitude of the bulk correlation length* ξ, provided $r_1/\xi^{(s)}$ is sufficiently large.

XI. DISCUSSION AND OUTLOOK

We have presented the global phase diagrams for wetting on spheres and cylinders in Landau theory. In our study, we examined the Landau theory with the standard quartic polynomial (2.2) by numerical methods, complemented with numerous analytical approximations and a fair amount of exact results. Our study was inspired by the numerical analysis of Levinson *et al.*[6] for the case $g = 0$. In later work Gelfand and Lipowsky[9] examined the case $g \neq 0$. They explored the regime of small curvature, $r_1 \gg \xi$. Furthermore, within this regime, they employed the double-parabola approximation to the Landau free energy. This approximation cannot be used near T_c and breaks down for $|g|\xi/c > \sqrt{2}$ (for $r_1 = \infty$).

Our findings do not support the previously reached conclusion that the effects of curvature may be subsumed into an effective bulk field.[9] Curvature and bulk field are similar in that both induce a finite wetting-layer thickness. However, the important difference is that when the strength of the bulk field is increased the prewetting transitions terminate at a critical point, whereas when the curvature is increased the adsorption phase transitions can behave in several different ways, depending on G (see Figs. 1 and 2). Even in the limit $r_1 \gg \xi$, we have not found a precise similarity between the roles of curvature and bulk field. The closest analogy to (8.2) is the following *approximate* result in the limit $r_1/\xi \to \infty$:

$$\frac{\bar{y}_1^2}{2} \approx (x_1^2-1)^2 m_b^2/c + p(2\sqrt{2}/3)(r_1/\xi)^{-1}(m_b^2/c) \times [|x_1-1|(x_1-1)(x_1+2)+4] , \quad (11.1)$$

with $p=1$ (cylinders) or $p=2$ (spheres). This result can be derived on the basis of (3.1) and with the use of an upper bound[19] for $|y_1(x_1)|$, as we shall outline below. In (11.1) we have defined $x(r)=m(r)/m_b$ and $\bar{y}(r)=-dx(r)/dr$ instead of the usual definitions in terms of $\rho=r/r_1$, in order to allow a direct comparison with (8.2).

In our study of the adsorption phase transitions we have emphasized that the knowledge of the curve of initial conditions $y_1(x_1)$ is essential. Often $y_1(x_1)$ is known only approximately. In such case, it is very useful to obtain lower and upper bounds for $|y_1(x_1)|$. For our problem the lower bound (4.23) is found immediately by noting that, in the mechanical analogy, energy is dissipated due to the presence of friction. Far less trivial is obtaining an upper bound. Consider, in the mechanical analogy, a particle with initial position x_1 and final position $x(\infty)=-1$. Then the velocity $y(x)$ at x (with $-1<x<x_1$ or $x_1<x<-1$) is less in magnitude than the initial velocity $y_1(x)$ which the particle would have for initial position x and the same final position -1. This can be written compactly as

$$|y(x)| \le |y_1(x)| . \quad (11.2)$$

This inequality can be shown analytically for small $x+1$, but we have only numerical evidence for the more general case. Using (11.2) and the fact that $\rho \ge 1$, in a relationship of the form (3.1), which describes the dissipation of mechanical energy, leads to

$$\frac{y_1^2}{2} - \frac{\Omega}{4}(x_1^2-1)^2 \le p \int_{-1}^{x_1} y_1(x)dx . \quad (11.3)$$

On the basis of (11.3), (11.1) is derived in the process of constructing successive approximations to $y_1(x_1)$ for large Ω. In the first iteration (replacing y_1 by its limit for $\Omega \to \infty$ in the integrand) one obtains (11.1).

The next topic of our discussion is the occurrence of critical double points in the phase diagrams (Figs. 1 and 2). At these points the regions of surface transitions and line (or point) transitions merge. Critical double points are well known in the context of bulk phase transitions. One example is the coincidence of the upper and lower consolute points in binary mixtures when pressure p and temperature T are varied.[20] The usual topology in such case consists of a critical line, projected in the (p,T) plane, which encloses a two-phase region. In our case the topology is *inverted* since the critical line encloses a one-phase region. An experimental example of this in bulk phase transition phenomena is found in the work of Trappeniers and Schouten[21] on mixtures of Neon and Krypton. From the point of view of critical phenomena, critical double points give rise to exponent doubling.[20,22]

As far as the experimental relevance of our results is concerned, we would like to make the following comments. The phase diagrams we presented are essential to experiments which deal with wetting on cylindrical wires or fibers,[23] and on spherical objects.[24] The continuum mean-field theory is expected to be primarily applicable to systems where both r_1 and ξ are appreciably larger than the molecular size. This size is represented in the Landau theory by the constant $\sqrt{c}$, where c is the coefficient of the gradient term in (2.1). Consequently, there are no restrictions on the ratio r_1/ξ, and the phase diagrams can be used to explain or predict adsorption phase transitions when the temperature is varied.

For a given choice of substrate r_1, h_1, and g are fixed. Without loss of generality we assume $h_1 > 0$ and the vapor phase for the adsorbate in bulk. When the temperature is raised from a sufficiently low value towards T_c, we will encounter a phase transition provided $G > G^*$, where G^* is the value of G at the critical double point. For $0 < G < G^*$, a phase transition will occur on the way to T_c unless h_1 falls within a certain range. A phase diagram in the $(H_1, r_1/\xi)$ plane which describes this regime is shown in our earlier paper.[12] For $G < 0$, a phase transition will take place unless h_1 is below a certain threshold value. These results can be stated in a different way. When T_c is approached at constant r_1, h_1, and g, a phase transition may but need not occur. Thus, the analog of *critical-point wetting*[1,3,25] on planar substrates (i.e., the necessity of a phase transition to complete wetting while T_c is approached from below) takes place only if $G > G^*$. Otherwise, h_1, for example, can be taken such that no phase transition occurs as T is raised towards T_c. (For $h_1 < 0$ the same discussion applies, replacing bulk vapor by bulk liquid and "wetting" by "drying").

Fluctuation effects will modify the phase diagrams. We have obviously neglected transverse fluctuations of the order parameter $m(\mathbf{r})$ by restricting its variation to the radial direction along r. We have also neglected local fluctuations of average size ξ, which are already present in the bulk phases at $r=\infty$. It remains to be investigated which topology the phase diagrams display beyond mean-field theory.

Concerning the finite-size rounding, we expect, on the basis of the arguments given in Sec. X, that this effect is not a limiting factor for experimental detection of the phase transitions, provided the radius r_1 is large compared to molecular sizes.

Inspired by this study of wetting on spheres and cylinders, we have begun to devote attention to other, more complicated substrate geometries. Examples are tori, paraboloids, and hyperboloids. Also gratings of parallel cylinders are being considered. The physical questions we address are the nature of the *connectivity phase transition* in which the emerging interface changes from singly to multiply connected (for example, on a torus, and between parallel cylinders), and the possibility of a *true wetting transition* on infinite rather than finite curved substrates (for example, on paraboloids). A technical problem in the treatment of the Landau theory for these geometries is the lack of a mechanical analogy (the "time" variable becomes two-dimensional), and, of course, the partial differential equations are harder to

deal with than the ordinary ones discussed here.

Another interesting problem which can be handled with the present methods is that of wetting at a planar wall, in the presence of a long-range substrate-adsorbate field $h(z)$, in Landau theory.[26,27] In the mechanical analogy the particle then moves under a time-dependent external force.

Finally, we would like to mention the widely relevant problem of wetting near grain boundaries and defect planes, for which the Landau theory allows an exact solution.[28] Also, concerning the widely applicable use of equal-areas rules, such as (3.2), in mathematical physics, we mention a recent review of generalized equal-areas rules for spatially extended systems.[29]

ACKNOWLEDGMENTS

P.J.U. acknowledges support from the Science and Engineering Research Council (United Kingdom) and the British Council. J.O.I. is grateful to B. Widom for valuable discussions and, in particular, for pointing out Ref. 21. He thanks the Belgian National Fund for Scientific Research for financial support.

APPENDIX: ANALYTIC APPROXIMATIONS FOR HIGH SUBSTRATE CURVATURE

A. Spheres

We perform a perturbative expansion of (2.10) in powers of Ω. If we consider

$$x(\rho)=x^{(0)}(\rho)+\Omega x^{(1)}(\rho)+\cdots \tag{A1}$$

with boundary conditions

$$x^{(0)}(1)=x_1,\quad x^{(n)}(1)=0,\quad n\geq 1\ , \tag{A2a}$$

$$-dx^{(0)}/d\rho|_{\rho=1}=y_1,\quad dx^{(n)}/d\rho|_{\rho=1}=0,\quad n\geq 1\ , \tag{A2b}$$

then we find

$$x^{(0)}(\rho)=x_1-y_1+y_1/\rho\ , \tag{A3}$$

$$\begin{aligned}x^{(1)}(\rho)=&-(\tfrac{1}{2}x_1^3-\tfrac{3}{2}y_1^3+\tfrac{3}{2}x_1^2y_1-\tfrac{3}{2}x_1y_1^2-\tfrac{1}{2}x_1+\tfrac{1}{2}y_1)+\frac{1}{\rho}(\tfrac{1}{3}x_1^3-\tfrac{17}{6}y_1^3+\tfrac{1}{2}x_1^2y_1+x_1y_1^2-\tfrac{1}{3}x_1-\tfrac{1}{6}y_1)\\&-y_1^3\ln\rho/\rho+(3x_1y_1^2-3y_1^3)\ln\rho+\tfrac{1}{2}\rho(3y_1^3+3x_1^2y_1-6x_1y_1^2-y_1)\\&+\tfrac{1}{6}\rho^2(x_1^3-y_1^3+3x_1y_1^2-3x_1^2y_1-x_1+y_1)\ .\end{aligned} \tag{A4}$$

From this first-order result one can construct a useful approximation to $y_1(x_1)$ as follows. First note that the expansion breaks down as $\rho\to\infty$, because, in first order, the boundary condition $x_\infty=-1$ cannot be satisfied. However, the expansion is useful provided

$$\Omega\rho^2<1\ . \tag{A5}$$

Since $\rho\geq 1$, the expansion will *a fortiori* be useful only for $\Omega<1$. From (A3) and (A4) we obtain $y(\rho)=-dx/d\rho$, and by substituting $y_1=H_1+Gx_1$ in both $x(\rho)$ and $y(\rho)$ one is led to the following third-degree polynomials:

$$x^{(0)}(\rho)+\Omega x^{(1)}(\rho)=\sum_{n=0}^{3}a_n(\rho,\Omega,H_1,G)x_1^n\ , \tag{A6}$$

$$y^{(0)}(\rho)+\Omega y^{(1)}(\rho)=\sum_{n=0}^{3}b_n(\rho,\Omega,H_1,G)x_1^n\ . \tag{A7}$$

On the other hand the asymptotic solution for $\rho\to\infty$ is found by linearizing (2.10) about $x=-1$ as in (4.1) for $P=0$. In this limit we have

$$x(\rho)\sim -1+\frac{A}{\rho}e^{-u\rho},\ \text{as}\ \rho\to\infty\ , \tag{A8}$$

where $u=(2\Omega)^{1/2}$. A can be eliminated by expressing $x(\rho)$ in terms of $y(\rho)$, which leads to

$$x(\rho)\sim -1+\rho y(\rho)/(u\rho+1),\ \text{as}\ \rho\to\infty\ . \tag{A9}$$

This suggests that one matches (A9) ("outer" solution[13]) with Eqs. (A3)–(A7) ("inner" solution), at $u\rho=1$ (or a suitable number of order 1). This leads to the following constraint,

$$\sum_{n=0}^{3}a_n(\rho=u^{-1},\Omega,H_1,G)x_1^n=-1+\frac{1}{2u}\sum_{n=0}^{3}b_n(\rho=u^{-1},\Omega,H_1,G)x_1^n\ . \tag{A10}$$

For fixed Ω, H_1, and G, Eq. (A10) can admit either one or three solutions for x_1, thus allowing an approximate location of the phase transition.

B. Cylinders

We expand (2.15) in powers of Ω. Consider

$$x(\rho)=x^{(0)}(\rho)+\Omega x^{(1)}(\rho)+\cdots \tag{A11}$$

subject to the boundary conditions

$$x^{(0)}(1)=x_1, x^{(n)}(1)=0,\ n\geq 1\ , \tag{A12}$$

$$-dx^{(0)}/d\rho|_{\rho=1}=y_1, dx^{(n)}/d\rho|_{\rho=1}=0,\ n\geq 1\ . \tag{A13}$$

We find

$$x^{(0)}(\rho)=x_1-y_1\ln\rho\ , \tag{A14}$$

$$x^{(1)}(\rho)=\tfrac{1}{4}(x_1+y_1-x_1^3-3x_1^2y_1-\tfrac{9}{2}x_1y_1^2-3y_1^3)+\tfrac{1}{4}\ln\rho(2x_1+y_1-2x_1^3-3x_1^2y_1-3x_1y_1^2-\tfrac{3}{2}y_1^3)$$
$$+\tfrac{1}{4}\rho^2(-x_1-y_1+x_1^3+3y_1^3+3x_1^2y_1+\tfrac{9}{2}x_1y_1^2)+\tfrac{1}{4}\rho^2\ln\rho(y_1-\tfrac{9}{2}y_1^3-3x_1^2y_1-6x_1y_1^2)$$
$$+\tfrac{1}{4}\rho^2(\ln\rho)^2(3y_1^3+3x_1y_1^2)+\tfrac{1}{4}\rho^2(\ln\rho)^3(-y_1^3)\ . \tag{A15}$$

On the basis of this first-order result one can construct a useful approximation to $y_1(x_1)$ as follows.

First note that the expansion is useless for $\rho\to\infty$. Already in zeroth order the boundary condition $x_\infty=-1$ cannot be satisfied for $y_1\neq 0$. The expansion is useful provided

$$\Omega\rho^2(\ln\rho)^3<1\ , \tag{A16}$$

From (A14) and (A15) we obtain $y(\rho)=-dx/d\rho$, and then substitute H_1+Gx_1 for y_1 in both $x(\rho)$ and $y(\rho)$. This leads to third-degree polynomials of the form (A6) and (A7).

On the other hand, for $\rho\to\infty$, we must have $x\to-1$, so that an expansion in $x+1$ as in (4.18) is the appropriate tool. We find

$$x(\rho)\sim -1+AK_0(u\rho)\ \text{ as } \rho\to\infty\ , \tag{A17}$$

where $u=(2\Omega)^{1/2}$. The coefficient A can be eliminated by expressing $x(\rho)$ in terms of $y(\rho)$:

$$x(\rho)\sim -1+K_0(u\rho)y(\rho)/[uK_1(u\rho)],\quad \rho\to\infty\ . \tag{A18}$$

Together with the foregoing results, this suggests a matching of the two expansions at $u\rho\approx 1$ [ignoring the logarithmic correction factor in (A16)]. This results in the following constraint on the initial condition x_1:

$$\sum_{n=0}^{3} a_n(\rho=u^{-1},\Omega,H_1,G)x_1^n = -1+\frac{K_0(1)}{uK_1(1)}\sum_{n=0}^{3} b_n(\rho=u^{-1},\Omega,H_1,G)x_1^n\ , \tag{A19}$$

with the desired one or three solutions x_1 for fixed Ω, H_1, and G.

*Present address: Institute for Physical Science and Technology, College Park, MD 20742.

[1]J. W. Cahn, J. Chem. Phys. **66**, 3667 (1977).

[2]C. Ebner and W. F. Saam, Phys. Rev. Lett. **38**, 1486 (1977).

[3]H. Nakanishi and M. E. Fisher, Phys. Rev. Lett. **49**, 1565 (1982).

[4]P.-G. de Gennes, Rev. Mod. Phys. **57**, 827 (1985).

[5]S. Dietrich, in *Phase Transitions and Critical Phenomena*, edited by C. Domb and J. Lebowitz (Academic, London, 1988), Vol. 12.

[6]P. Levinson, J. Jouffroy, and F. Brochard, J. Phys. (Paris) Lett. **46**, L21 (1985).

[7]F. Brochard, J. Chem. Phys. **84**, 4664 (1986).

[8]R. Holyst and A. Poniewierski, Phys. Rev. B **36**, 5628 (1987); Physica A **149**, 622 (1988).

[9]M. P. Gelfand and R. Lipowsky, Phys. Rev. B **36**, 8725 (1987).

[10]P.-G. de Gennes, C. R. Acad. Sci. Paris II **297**, 9 (1983).

[11]M. P. Nightingale and J. O. Indekeu, Phys. Rev. B **32**, 3364 (1985).

[12]J. O. Indekeu, P. J. Upton, and J. M. Yeomans, Phys. Rev. Lett. **61**, 2221 (1988).

[13]D. W. Jordan and P. Smith, *Nonlinear Ordinary Differential Equations* (Clarendon, Oxford, 1987).

[14]J. W. Schmidt and M. R. Moldover, J. Chem. Phys. **84**, 4563 (1986).

[15]J. W. Schmidt, J. Colloid Interface Sci. **122**, 575 (1988).

[16]V. Privman and M. E. Fisher, J. Stat. Phys. **33**, 385 (1983); J. Appl. Phys. **57**, 3327 (1985).

[17]D. B. Abraham, Phys. Rev. Lett. **44**, 1165 (1980).

[18]In order to demonstrate the algebraic decay, it suffices to note that $x(\rho)=\omega^{-1/2}/\rho$ is a (special) solution of Eq. (6.10).

[19]J. O. Indekeu, Nucl. Phys. B **5A**, 168 (1988).

[20]R. E. Goldstein and J. S. Walker, J. Chem. Phys. **78**, 1492 (1983), and references therein.

[21]N. J. Trappeniers and J. A. Schouten, Physica **73**, 546 (1974).

[22]R. G. Johnston, N. A. Clark, P. Wiltzius, and D. S. Cannell, Phys. Rev. Lett. **54**, 49 (1985).

[23]P. Taborek and L. Senator, Phys. Rev. Lett. **57**, 218 (1986).

[24]D. Beysens and D. Estève, Phys. Rev. Lett. **54**, 2123 (1985).

[25]For experiments on wetting phase transitions arbitrarily close to T_c, see L. Sigl and W. Fenzl, Phys. Rev. Lett. **57**, 2191 (1986).

[26]V. Privman, J. Chem. Phys. **81**, 2463 (1984).

[27]G. Langie and J. O. Indekeu Phys. Rev. B (to be published).

[28]A. Sevrin and J. O. Indekeu, Phys. Rev. B **39**, 4516 (1989).

[29]E. Schöll and P. T. Landsberg, Z. Phys. B **72**, 515 (1988).